



# Dual-Core Liquid Filled Photonic Crystal Fiber Coupler

Md. Bellal Hossain<sup>1</sup>, Md. Mahbub Hossain<sup>1\*</sup>, Md. Ekhlalur Rahaman<sup>1</sup>, Md. Younus Ali<sup>1</sup> and Himadri Shekhar Mondal<sup>1</sup>

<sup>1</sup>Electronics and Communication Engineering Discipline, Khulna University, Khulna-9208, Bangladesh

\*Corresponding author E-mail: [mahbub.eceku@yahoo.com](mailto:mahbub.eceku@yahoo.com)/[mahbub.hossain@ece.ku.ac.bd](mailto:mahbub.hossain@ece.ku.ac.bd), phone: +8801712633067

## Abstract

Photonic crystal fiber coupler (PCFC) is one of the remarkable devices that contribute a key responsibility in passive optical networks and enormous optical systems. This paper presents a dual-core liquid filled PCFC with rectangular and hexagonal geometry for analyzing different guiding properties from 1200 to 1800 nm wavelength range by finite difference time domain (FDTD) method with transparent boundary condition (TBC). In the proposed design, the background material (Silica and BK7) and the liquid (water, chloroform, benzene) in the dual-core are varied. Results imply very small confinement loss with low coupling length for wide wavelength range. At 1.55  $\mu\text{m}$  wavelength, hexagonal PCFC (Silica) shows 0.00025, 0.00051, and 0.00095 m coupling length for water, chloroform, and benzene infiltrated dual-core, respectively. As well, the confinement loss of  $1.655 \times 10^{-8}$ ,  $0.84 \times 10^{-8}$ , and  $0.739 \times 10^{-8}$  dB/km and the birefringence of  $3.08 \times 10^{-4}$ ,  $1.48 \times 10^{-4}$ , and  $0.801 \times 10^{-4}$  are obtained in water, chloroform, and benzene filled dual-core, correspondingly. Furthermore, at 1.55  $\mu\text{m}$  wavelength benzene exhibits the maximum polarization-insensitivity for the both the PCFC structures. In addition, the proposed PCFCs demonstrate high coupling coefficient with ultra flattened dispersion for broad wavelength range.

**Keywords:** Birefringence; Coupling length; Confinement loss; Photonic crystal fiber coupler (PCFC); Polarization-insensitivity; Propagation constant.

## 1. Introduction

Photonic crystal fiber (PCF) is a special class of optical fiber that has a great impact on communication field with high-speed data transmission [1, 2]. It is well known that telecommunication window (approximately 1.55  $\mu\text{m}$ ) is the key area in optical communication, dispersion compensation fiber (DCF) and nonlinear optics. This is due to the minimum transmission loss of the fiber in this area [3–5]. PCFs have explored novel traditions to control the light due to its new guiding characteristics like splitters, twin-core couplers, de-multiplexers, and ring-laser cavities [6–9]. Moreover, it has different potential applications [10]. PCFs based on pure Silica show amazing modal characteristics like single mode operation at a small operating wavelength, remain single mode for large-scale fibers, achieve high birefringence, and convenient dispersion characteristics which cannot be achieved with conservative optical fibers [11–13]. Nowadays, PCFs have exhibited a broad range of important optical properties which was not possible to attain by traditional fiber technology [2]. A conventional PCF having Silica core with numerous air-holes arranged periodically in cladding region shows high non linearity [9]. In conventional optical fiber, light propagates through it using total internal reflection (TIR) concept and the core material has larger refractive index than the cladding material to create the situation of TIR. However, this is not the scenario for the propagation of light in PCFs [7]. The cladding region is changed by creating micro-structures to prevent light not to propagate there. The effective refractive index is an important property for PCF which has related to the calculation of different parameters of optical communication. This index is varied with the wavelength of light in PCF and this vari-

ation is important for defining optical properties such as dispersion, confinement loss, coupling length, birefringence etc. [14].

The dominant wavelength reliance on the refractive index and naturally great design suppleness of the PCFs have a great effect with inventive properties [11]. Also, the variation of PCFs structure show significant effect on the optical properties. In addition, within a fixed wavelength range the effective refractive index is changed [15–17]. By changing its internal structure of PCFs, the confinement loss, coupling length, coupling coefficient, and birefringence can be re-engineered [17]. PCF couplers (PCFCs) support a lot of stimulating light-guiding features when compared to the traditional optical fiber coupler [18]. Different internal structural parameters like air hole diameter, lattice pitch, inter-core separation, and radius have shown significant impact not only on the coupling length but also birefringence, confinement loss, and dispersion [19–21]. The propagating evanescent mode of light is moved to the adjacent core in a dual-core PCFC [22]. Dual-core PCFCs have numerous benefits further than traditional optical couplers for example extra supple design and smaller coupling length. Recently, a hexagonal lattice PCFC presented coupling length of 0.0006, 0.0008, and 0.007 m respectively for silica, chloroform, and benzene filled dual-core at 1.55  $\mu\text{m}$  wavelength [18]. However, to reduce the coupling length the air-hole diameter is optimized which introduces fabrication complexity and also polarization effect that are not analyzed.

To optimize the PCFC guiding properties, the operating wavelength, PCF geometry, and liquid in the dual-core is varied. As a result, the effective refractive index varies accordingly. Thus, the coupling length and coefficient, dispersion, birefringence, and confinement loss is changed [18]. To understand the effect of changing the struc-

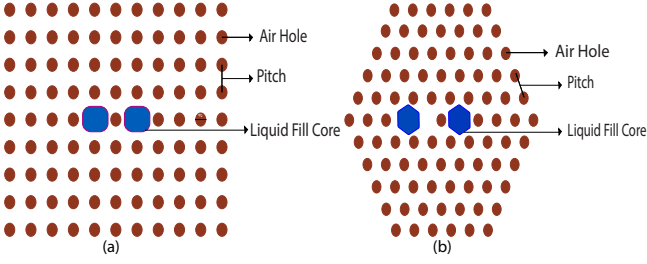


**Figure 1:** Design layout of rectangular and hexagonal PCFCs (a) rectangular PCFC, and (b) hexagonal PCFC.

ture parameters, background materials, and liquids through the core region on the coupling length and others properties can be analyzed and compared. As a result, better PCF coupler can be developed. In this paper, the coupling length along with the birefringence and confinement loss for liquid-filled PCFs are investigated. There are small number of published papers which analyze the different optical properties of different PCFC geometries by inserting liquid in the dual-core [23]. Therefore, there is still scoping to design new structure of PCFC with different background materials individually and analyze their light properties by inserting different types of liquid through the core region. In the proposed design, four rings of rectangular and hexagonal geometry PCFC are considered for analyzing coupling length and coefficient, effective refractive index, propagation constant, confinement loss, dispersion, and birefringence from 1200 to 1800 nm wavelength range applying finite difference time domain (FDTD) through transparent boundary condition (TBC).

## 2. PCF Coupler Design and Theory

In this report, a dual-core rectangular and hexagonal PCFC is proposed. The desire of the proposed study is to get wide-band wavelength dullness, polarization insensitive, and low confinement loss which can be spliced through single-mode fiber in a small inserted loss. Though the main goal is reducing the coupling length. Two different materials like Silica ( $n = 1.46$ ) and BK7 ( $n = 1.506$ ) are used as background material separately. Also, the core region is filled with different liquids such as water (1.33), chloroform (1.445) and benzene (1.501). The cross-section of the proposed dual-core PCFCs are exposed in Figure. 1. The cores are recognized through intentionally absent air-hole on the Silica or BK7 substrate. In the proposed design, four rings of air-holes are used to form the cladding with each air-hole diameter is taken  $d_1=0.6 \mu\text{m}$ . Moreover, the distance between two air-hole which is usually called lattice pitch is,  $\Lambda = 2.3 \mu\text{m}$ . In addition, each hole diameter of dual-core,  $d_c = 0.4 \mu\text{m}$  is considered where inter-core separation is  $4.6 \mu\text{m}$  ( $2\Lambda$ ). A point source is used as a light source in the core which has wide-band wavelength range. The rectangular and hexagonal PCFC optical field confinement is observed in Figure. 2.

The optical field distribution and effective refractive index of the proposed PCFCs are computed applying FDTD method. The cladding layers are shaped with allocating the circular air-holes in a hexagonal or rectangular lattice. After simulating these proposed PCFC models the effective refractive index is obtained. The effective mode index is calculated using the eigenvalue problem of Maxwell's equation. Moreover, effective refractive index is derived by solving Maxwell's vectorial equations [24]

$$\nabla \times ([s]^{-1} \nabla \times E) - k_0^2 n^2 [s] E = 0 \quad (1)$$

where  $s$  and  $s^{-1}$  are scattered and inversely scattered matrix accordingly,  $k_0$  is the free space wave number,  $\lambda$  is wavelength,  $n$  is the effective refractive index and  $E$  is electric field vector. The propagation constant of an electromagnetic signal is the variation of the amplitude spreads in a given direction. Therefore, the propagation

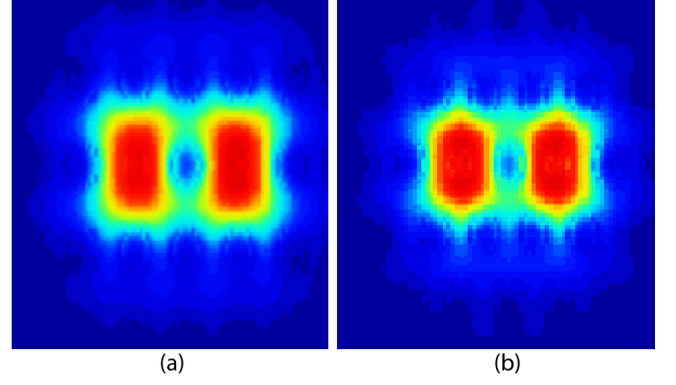


**Figure 2:** Field confinement of rectangular and hexagonal PCFCs (a) rectangular PCFC (x-polarization), (b) hexagonal PCFC (y-polarization).

constant of an electromagnetic wave is given by the equation [18]

$$\beta = n_{eff} \frac{2\pi}{\lambda} \quad (2)$$

where  $n_{eff}$  is the effective refractive index. The dispersion coefficient is calculated by [25]

$$D = -\frac{\lambda}{c} \frac{d^2}{d\lambda^2} n_{eff} \quad (3)$$

where  $c$  is the speed of light. Also, confinement loss which is related with the imaginary part of effective refractive index and can be computed [4]

$$CL = 8.686 \times 10^3 (2\pi/\lambda) \text{Im}(n_{eff}) \text{dB/km} \quad (4)$$

Here,  $\text{Im}(n_{eff})$  is the effective refractive index (imaginary). Coupling length is the space that supports the transfer of light from one guided mode to the further by evanescent waves. However, coupler length generally depends on the inter-core separation, transmitting wavelength and core diameter. The coupling length is given by [18]

$$L_c = \lambda / (2 | n_{even} - n_{odd} |) \quad (5)$$

$n_{even}$  and  $n_{odd}$  are the effective refractive indexes of even and odd polarization modes, correspondingly. Moreover, coupling coefficient is calculated by [25]

$$k_0 = 2L_c / \pi \quad (6)$$

The birefringence is obtained through the real part of effective refractive index difference of two vital polarization modes which can be written as [23]

$$B = | n_{eff}^x - n_{eff}^y | \quad (7)$$

where  $n_{eff}^x$  and  $n_{eff}^y$  is the effective refractive index for x and y-polarization, respectively.

## 3. Results and Discussion

It is well known that the speed of light through any material increases with the raising of wavelength. So, with the increase of wavelength, the refractive index of any material decreases. Figure. 3 shows the effective refractive index with respect to wavelength with different background materials like Silica and BK7 for rectangular PCFC structure. Again, for each background material the liquid for example water, chloroform, and benzene are filled in the dual-core. Generally, increasing wavelength the effective refractive index is decreased. Moreover, benzene shows the highest index for both the background materials. Figure. 4 represents the effective refractive index with respect to wavelength for hexagonal PCFC model. In this proposed model, similar background materials and liquids in the dual-core are

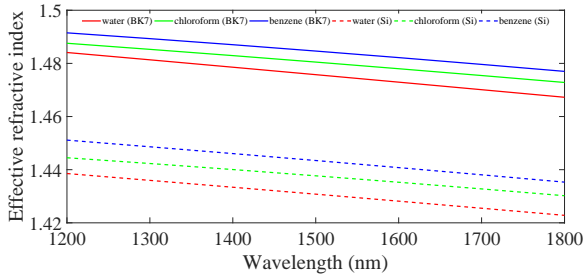


**Figure 3:** Variation of the effective refractive index with respect to wavelength for rectangular PCFC geometry (x-polarization). Solid line presents BK7 where dashed line shows Silica.

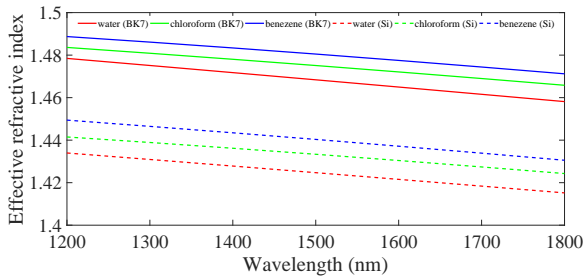
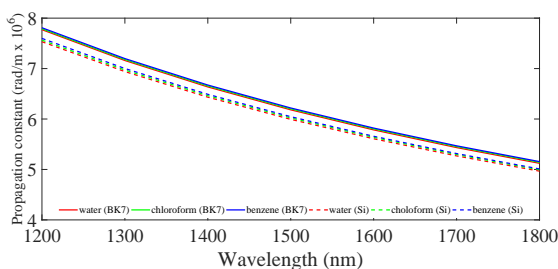


**Figure 4:** Variation of the effective refractive index with respect to wavelength for hexagonal PCFC geometry (y-polarization). Solid line presents BK7 where dashed line shows Silica.

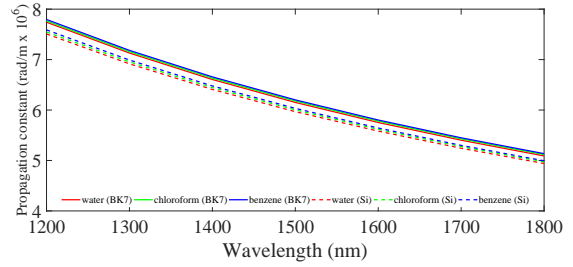
applied. Silica exhibits the higher rate of reduction of the effective refractive index compared to BK7. Moreover, among the three materials, the refractive index is comparatively small when core region is filled with water.

Figure. 5 and 6 show the variation of the propagation constant with respect to wavelength for rectangular and hexagonal PCFCs geometry. Propagation constant decreases with the increasing of wavelength for both structures and for all the three liquids filled in the core region. For smaller wavelength, the propagation constant is straightly relative to the effective mode index and found to be highest. Increasing wavelength, the propagation constant reduces with respect to the effective mode index. For both structures, propagation constant is seemed high for BK7, comparatively. Propagation constant is approximately  $7.89 \text{ (rad/m} \times 10^6)$  for BK7 and  $7.48 \text{ (rad/m} \times 10^6)$  for Silica glass material at 1200 nm. However, at 1800 nm wavelength these constant is reduced to  $5.25 \text{ (rad/m} \times 10^6)$  and  $5.01 \text{ (rad/m} \times 10^6)$  for BK7 and Silica, respectively. The rate of reduction of the propagation constant is 7.33% and 6.86% for BK7 and Silica, accordingly for every 100 nm wavelength. The highest propagation constant is observed for benzene and lowest for water. However, the variation of propagation constant of these three liquids is shown very small.

Figure. 7 (a) and (b) represent the variation of confinement loss



**Figure 5:** Variation of the propagation constant with respect to wavelength for rectangular PCFC geometry. Solid line presents BK7 where dashed line shows Silica.



**Figure 6:** Variation of the propagation constant with respect to wavelength for hexagonal PCFC geometry. Solid line presents BK7 where dashed line shows Silica.

with respect to wavelength for rectangular PCFC geometry with two different background materials. It is noted that confinement loss enhances with the increasing of wavelength. Also, confinement loss behaves approximately similar tendency for both of the background materials. In addition, Figure. 8 (a) and (b) show the variation of confinement loss with respect to wavelength for hexagonal PCFC geometry. High confinement loss is shown when core region is filled with water and low confinement loss is found when the core is filled with benzene. Also, low confinement loss is observed for BK7 and Silica material for rectangular and hexagonal PCFC, accordingly. At  $1.55 \mu\text{m}$  wavelength and BK7 background material, the lowest  $1.128 \times 10^{-8}$  and  $1.383 \times 10^{-8}$  dB/km confinement loss are obtained for rectangular and hexagonal PCFC, respectively with benzene liquid. For the similar condition, at Silica-based background material, benzene exhibits the lowest loss for rectangular PCFC model.

Table. 1 shows the comparison of confinement loss at  $1.55 \mu\text{m}$  wavelength for both the PCFCs. Results imply that when Silica is used as the background material then hexagonal PCFC presents lowest confinement loss for each type of liquids filled in the dual-core. Moreover, the lowest confinement loss  $0.739 \times 10^{-8}$  dB/km is observed for benzene at  $1.55 \mu\text{m}$  wavelength with hexagonal geometry. These results also demonstrate that the electric field is strongly confined in the core region for hexagonal PCFC. In addition, Silica-based PCFC with hexagonal geometry shows the lowest confinement loss from the broad wavelength range.

Figure. 9 (a) and (b) show the variation of coupling length with respect to wavelength for rectangular PCFC geometry. Also, Figure. 10 (a) and (b) represent the variation of coupling length with respect to wavelength for hexagonal PCFC geometry. The coupling length is shown to be large for small wavelength for both PCFC structures. It is expected that as the wavelength increases, the mode field expands and the coupling between the dual-core is decreased. Therefore, the coupling length reduces with the increase of wavelength. However, in Figure. 10 one can see that this behavior is not fully met. For benzene (Si), the coupling length at 1500 nm is smaller than the coupling length at 1600 nm. Coupling length decreases by increasing the effective core area, due to enhancing the inter-core separation [26]. Generally, increasing wavelength the field confinement is scattered. As a result, the effective core area is increased which confirms small coupling length. It is reported that  $d_c/\lambda$  has a great impact on coupling length and when this ratio is less than 0.42 then coupling length is decreased with increasing wavelength [27]. When core is filled with water then coupling length is comparatively small for both the background materials. Chloroform and benzene show higher coupling length than water due to higher refractive index. Moreover, using Silica as the background material the rate of reduction of coupling length for water is comparatively smaller than the other liquids. The similar tendency is observed for the PCFC model. However, the rate of reduction of coupling length is severer for benzene. For hexagonal BK7 PCFC structure, the rate of reduction for every 100 nm wavelength is 13.33%, 7%, and 3.03% for benzene, chloroform, and water liquid filled in the dual-

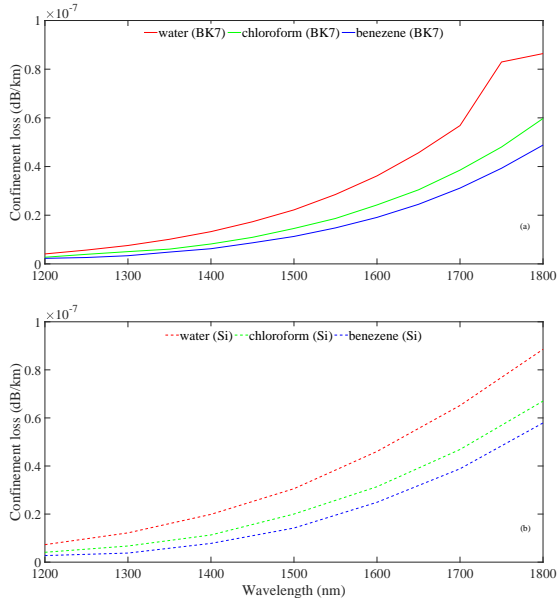


**Figure 7:** Variation of the confinement loss with respect to wavelength for rectangular PCFC geometry (a) BK7, and (b) Silica.

core. Noted that, this reduction rate is almost similar to other PCFC structure (rectangular).

In Table. 2, the comparison of coupling length is given at  $1.55 \mu\text{m}$  wavelength range. The lowest coupling length  $0.00025 \text{ m}$  is found for hexagonal PCFC at Silica background material when the dual-core is infiltrated by water. Again, at  $1.55 \mu\text{m}$  wavelength rectangular PCFC model with BK7 background material shows  $0.00040$ ,  $0.00046$ , and  $0.00052 \text{ m}$  coupling length. Also, the minimum coupling length of water, chloroform, and benzene are  $0.00025$ ,  $0.00046$ , and  $0.00052 \text{ m}$ , accordingly for different geometry and background materials. In addition, Silica-based PCFC (hexagonal) model exhibits  $0.00025$ ,  $0.00051$ , and  $0.00095 \text{ m}$  coupling length for water, chloroform, and benzene, respectively. So far, this is the lowest coupling length compared to existing work [18].

Figure. 11 (a) and (b) show the variation of coupling coefficient with respect to wavelength for rectangular PCFC geometry. Also, Figure. 12 (a) and (b) represent the disparity of coupling coefficient with respect to wavelength for hexagonal PCFC geometry. Coupling coefficient is observed usually short to the lower wavelength for both PCFC structures. However, with the increasing of wavelength, this coefficient is enhanced. When the core is filled with water then coupling coefficient is maximum for both the background materials due to minimum coupling length. Chloroform and benzene show comparatively small coupling coefficient than water due to higher refractive index. In Table. 3, the comparison of coupling coefficient is given at  $1.55 \mu\text{m}$  wavelength range. The highest coupling coefficient  $3748.5$ ,  $4354$ ,  $2187$ , and  $5979 \text{ m}^{-1}$  is observed for water filled dual-core PCFC for both the background materials and structures. Again, at  $1.55 \mu\text{m}$  wavelength hexagonal PCFC model with Silica background material and water infiltrated dual-core shows the maximum coupling coefficient with minimum length. In addition, Silica-based PCFC (hexagonal) model exhibits  $5979$ ,  $3026$ , and  $1599 \text{ m}^{-1}$  coefficient for water, chloroform, and benzene, respectively.

Figure. 13 (a) and (b) show the variation of birefringence with respect to wavelength for rectangular and Figure. 14 (a) and (b) represent hexagonal geometry. As shown in these figures, birefringence increases with the raises of wavelength. Water shows large birefringence for all these PCFC model except rectangular PCFC with Silica background material. Figure. 13 (b) illustrates that the birefringence is decreased after  $1600 \text{ nm}$  for benzene and  $1700 \text{ nm}$  for chloroform. In Table. 4, the comparison of birefringence is shown at  $1.55 \mu\text{m}$  wavelength. At  $1.55 \mu\text{m}$  wavelength, the highest

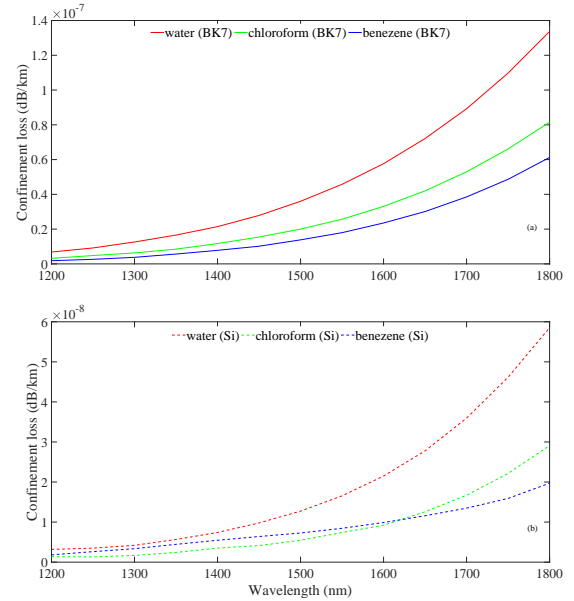


**Figure 8:** Variation of the confinement loss with respect to wavelength for hexagonal PCFC geometry (a) BK7, and (b) Silica.

birefringence is obtained  $3.08 \times 10^{-4}$ ,  $1.62 \times 10^{-4}$ , and  $1.87 \times 10^{-4}$  for water, chloroform and benzene, respectively. The condition to get high birefringence is the difference of effective refractive index between two fundamental modes polarized in x and y-direction. Among the three different liquids, chloroform shows the minimum value of birefringence. A slight change of birefringence confirms the polarization insensitivity, thus it may be conclude that chloroform shows the polarization independence. To intricate the polarization insensitive uniqueness, the refractive index difference between x and y-polarization is introduced. As the proposed PCFC shows ultra small index difference and also the changing rate for every  $100 \text{ nm}$  wavelength is approximately  $0.13 \times 10^{-4}$  which confirms the polarization insensitivity. Moreover, benzene exhibits the maximum polarization independence behavior.

In Table. 3, the comparison of coupling coefficient is given at  $1.55 \mu\text{m}$  wavelength range. The highest coupling coefficient  $3748.5$ ,  $4354$ ,  $2187$ , and  $5979 \text{ m}^{-1}$  is observed for water filled dual-core PCFC for both the background materials and structures. Again, at  $1.55 \mu\text{m}$  wavelength hexagonal PCFC model with Silica background material and water infiltrated dual-core shows the maximum coupling coefficient with minimum length. In addition, Silica-based PCFC (hexagonal) model exhibits  $5979$ ,  $3026$ , and  $1599$  coefficient for water, chloroform, and benzene, respectively. Results depict significant improvement of coupling coefficient from the existing literature [25]. In Table. 4, the comparison of birefringence is shown at  $1.55 \mu\text{m}$  wavelength range. Chloroform exhibits the minimum birefringence for different PCFCs model and background material. However, rectangular PCFC with Silica background material presents the minimum birefringence when the core is filled any types of liquids.

The calculation of the dispersion for proposed PCFC models requires vast well-organized numerical techniques. As the dispersion is dependent on the second derivative of the effective refractive index with respect to the wavelength, thus the accuracy of  $n_{eff}$  with respect to wavelength is vital. Figure. 15 (a) and (b) represent the variation of dispersion with respect to wavelength for rectangular PCFC geometry. Also, Figure. 16 (a) and (b) exhibit the variations of dispersion with respect to wavelength for hexagonal PCFC geometry. Generally, dispersion value decreases minutely for rectangular PCFC with the two materials and liquids filled in the dual-core. However, hexagonal PCFC shows almost stable dispersion values from  $1200$  to  $1800 \text{ nm}$  wavelength range. In Figure. 16 (b), water demonstrates the constant dispersion from large wavelength range. The dispersion

**Table 1:** Comparison of the confinement loss (dB/km) at 1.55 μm wavelength of the proposed PCFC

	Rectangular PCFC (BK7)	Hexagonal PCFC (BK7)	Rectangular PCFC (Si)	Hexagonal PCFC (Si)
Water	$2.2 \times 10^{-8}$	$3.602 \times 10^{-8}$	$3.05 \times 10^{-8}$	$1.655 \times 10^{-8}$
Chloroform	$1.455 \times 10^{-8}$	$2 \times 10^{-8}$	$2 \times 10^{-8}$	$0.84 \times 10^{-8}$
Benzene	$1.128 \times 10^{-8}$	$1.383 \times 10^{-8}$	$1.419 \times 10^{-8}$	$0.739 \times 10^{-8}$

**Table 2:** Comparison of coupling length (m) at 1.55 μm wavelength of the proposed PCFC

	Rectangular PCFC (BK7)	Hexagonal PCFC (BK7)	Rectangular PCFC (Si)	Hexagonal PCFC (Si)
Water	0.00040	0.00035	0.00068	0.00025
Chloroform	0.00046	0.00064	0.00090	0.00051
Benzene	0.00052	0.00095	0.00091	0.00095

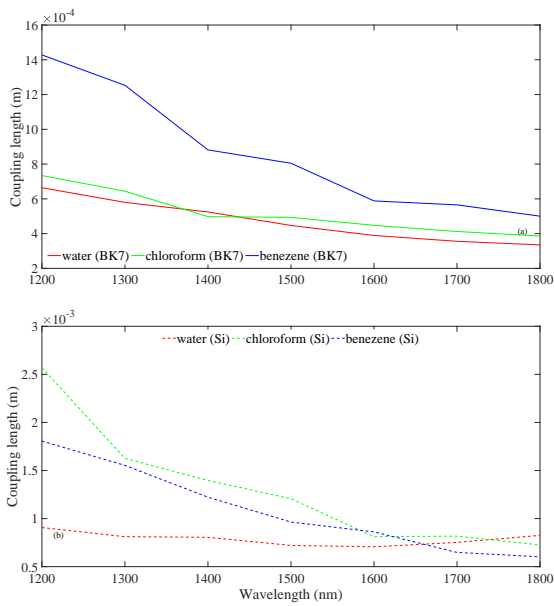


**Figure 9:** Variation of coupling length with respect to wavelength for rectangular PCFC geometry (a) BK7, and (b) Silica.

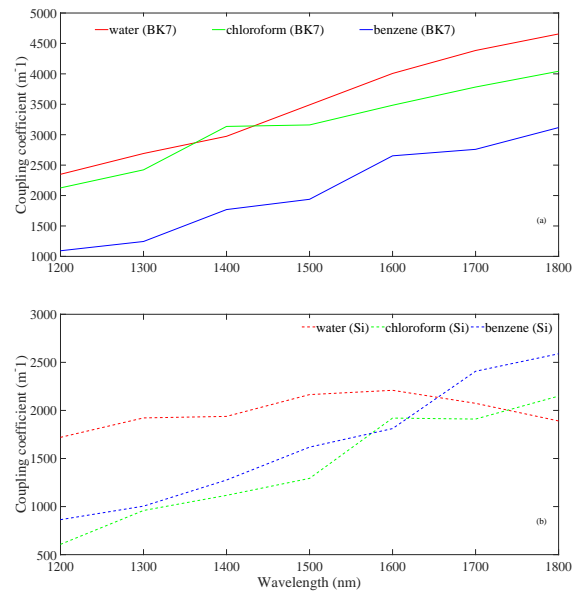


**Figure 11:** Variation of coupling coefficient with respect to wavelength for rectangular PCFC geometry (a) BK7, and (b) Silica.

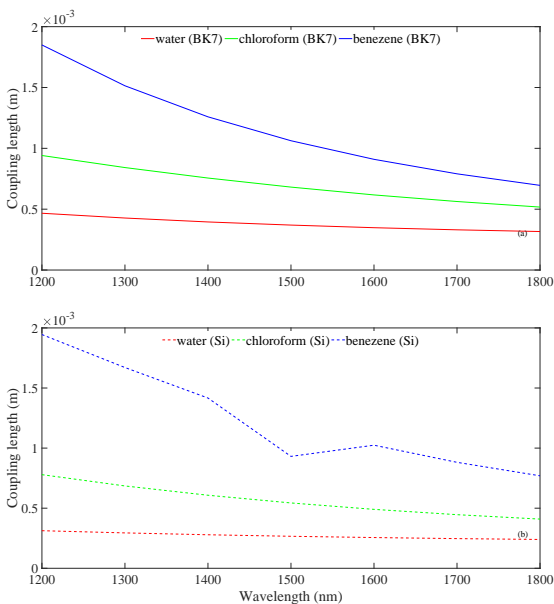


**Figure 10:** Variation of coupling length with respect to wavelength for hexagonal PCFC geometry (a) BK7, and (b) Silica.

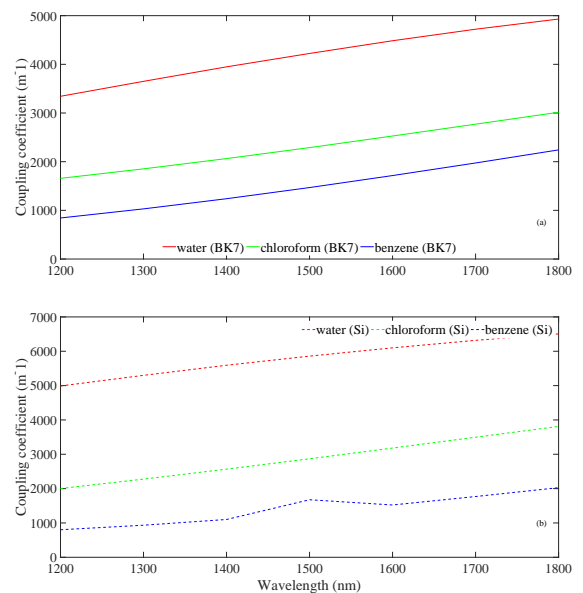


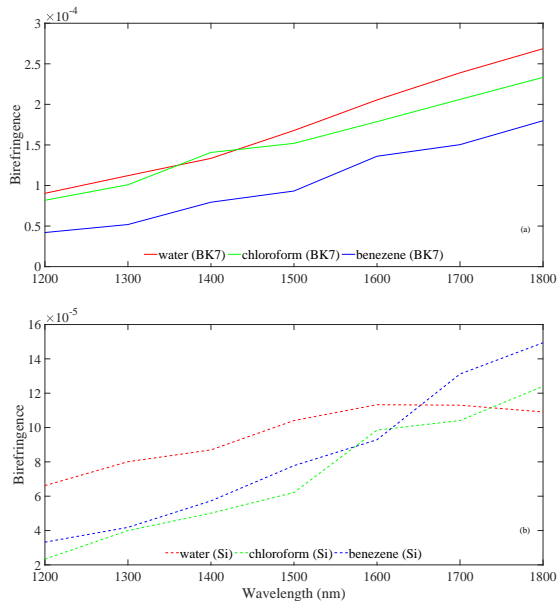
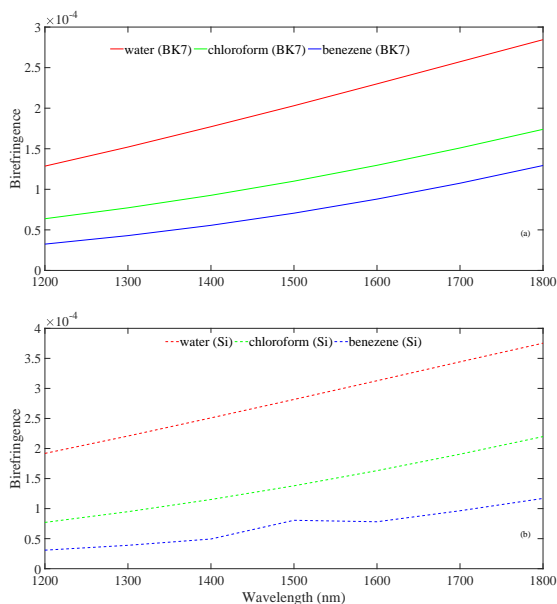
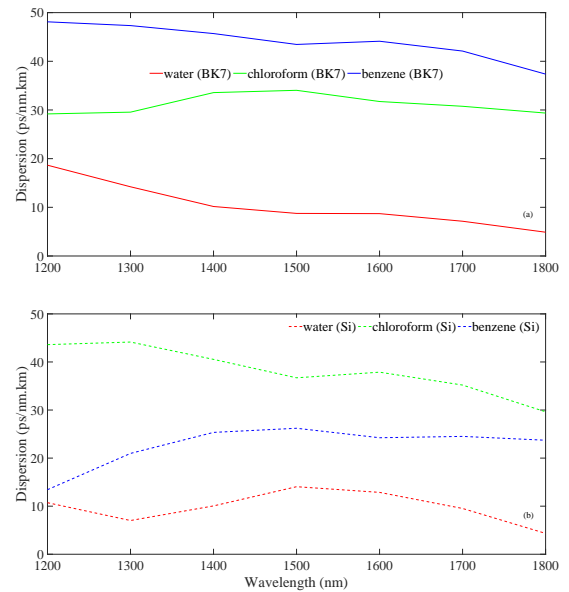
**Figure 12:** Variation of coupling coefficient with respect to wavelength for hexagonal PCFC geometry (a) BK7, and (b) Silica.

**Table 3:** Comparison of coupling coefficient ( $\text{m}^{-1}$ ) at  $1.55 \mu\text{m}$  wavelength of the proposed PCFC

	Rectangular PCFC (BK7)	Hexagonal PCFC (BK7)	Rectangular PCFC (Si)	Hexagonal PCFC (Si)
Water	3748.5	4354	2187	5979
Chloroform	3322.5	2408	1606.5	3026
Benzene	2295.5	1591.5	1714	1599

**Table 4:** Comparison of birefringence at  $1.55 \mu\text{m}$  wavelength of the proposed PCFC

	Rectangular PCFC (BK7)	Hexagonal PCFC (BK7)	Rectangular PCFC (Si)	Hexagonal PCFC (Si)
Water	$1.8 \times 10^{-4}$	$2.10 \times 10^{-4}$	$1.09 \times 10^{-4}$	$3.08 \times 10^{-4}$
Chloroform	$1.62 \times 10^{-4}$	$1.21 \times 10^{-4}$	$0.75 \times 10^{-4}$	$1.48 \times 10^{-4}$
Benzene	$1.87 \times 10^{-4}$	$0.78 \times 10^{-4}$	$0.95 \times 10^{-4}$	$0.801 \times 10^{-4}$

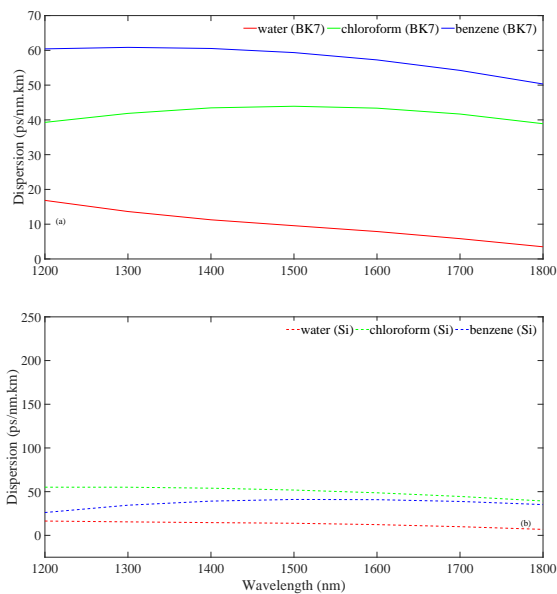
**Figure 13:** Variation of birefringence with respect to wavelength for rectangular PCFC geometry (a) BK7, and (b) Silica.**Figure 14:** Variation of birefringence with respect to wavelength for hexagonal PCFC geometry (a) BK7, and (b) Silica glass.**Figure 15:** Variation of dispersion with respect to wavelength for rectangular PCFC geometry (a) BK7, and (b) Silica glass.

variation is only  $10 \text{ ps/nm.km}$  for wide wavelength range. So, the proposed PCFC can be utilized in broadband wide-division multiplexing (WDM). The reason behind these characteristics is the slight variation of the effective index (real) with respect to wavelength. In addition, chloroform shows the similar behavior at the same wavelength range with slightly better dispersion value. However, the dispersion variation is observed smaller than water ( $5 \text{ ps/nm.km}$ ). In addition, Table. 5 shows the comparison of dispersion at  $1.55 \mu\text{m}$  wavelength. Structure variation does not affect the dispersion property when water is infiltrated in the dual-core. However, chloroform and benzene show the dispersion shifting behavior due to structure variation. As dispersion is significantly related to effective refractive index then it is increasing positively by changing the liquids in the dual-core.

Furthermore, PCFC with BK7 (background material), chloroform shows extremely low dispersion variation for large wavelength range. Result demonstrates only  $1 \text{ ps/(nm.km)}$  dispersion variation from  $1200$  to  $1800 \text{ nm}$  wavelength range. Therefore, from this dispersion analysis, it is noted that the proposed PCFC shows small dispersion variation which is very much essential for long distance data transmission. Likewise, these PCFCs through virtually ultra-flattened dispersion have a comparatively low effective mode area and also can be applied to the super-continuum generation, soliton pulse transmission, and so on [28]. As the lattice pitch is  $2.3 \mu\text{m}$  and fill fraction ratio ( $0.26$ ) is very small then it is attainable to get a closely ultra-flattened positive dispersion PCF in the telecommunication window. The previous study proved the positive dispersion is

**Table 5:** Comparison of dispersion (ps/nm.km) at 1.55  $\mu\text{m}$  wavelength of the proposed PCFC

	Rectangular PCFC (BK7)	Hexagonal PCFC (BK7)	Rectangular PCFC (Si)	Hexagonal PCFC (Si)
Water	8.72	8.72	13.46	13.07
Chloroform	32.89	43.64	37.29	50.27
Benzene	43.79	58.30	25.22	40.96

**Figure 16:** Variation of dispersion with respect to wavelength for hexagonal PCFC geometry (a) BK7, and (b) Silica glass.

achieved when the fill fraction ratio is 0.26 [29]. However, one of the reasons behind of positive dispersion is the very low effective refractive index difference as shown in Figure. 3 and 4. Some reports illustrated the reason for positive dispersion due to the maximum curvature of the effective index [30]. On the other hand, lattice pitch has significant effects on positive dispersion [29].

#### 4. Conclusion

Instantaneous attainment of low coupling length and confinement loss, small birefringence changes for wide wavelength range and flat normal dispersion for PCFC would offer a novel podium for optical fiber communication and sensing system. In this report, four rings dual-core PCFC for both rectangular and hexagonal geometry is proposed. Also, two different background materials and three different liquids (filled in dual-core) are used from 1200 to 1800 nm wavelength range. Various guiding properties like propagation constant, confinement loss, birefringence, coupling length and coefficient, and dispersion are investigated and compared. The proposed PCFC structures show ultra small confinement loss and coupling length at 1.55  $\mu\text{m}$  wavelength. Moreover, at this particular wavelength, the birefringence value is very small which confirms the polarization insensitivity. It may conclude that the dual-core Silica based hexagonal PCFC shows lowest coupling length than the existing literature which has hopeful potential in polarization independence sensing applications. However, it is required to optimize the structure parameters to further decreasing of the coupling length.

#### References

- [1] P. Agarwal, Modeling of elliptical air hole pcf for lower dispersion, *Advance in Electronic and Electric Engineering* 3 (2013) 439–446.
- [2] H. Ademgil, Highly sensitive octagonal photonic crystal fiber based sensor, *Optik-International Journal for Light and Electron Optics* 125 (20) (2014) 6274–6278.
- [3] F. Begum, Y. Namihira, A. SM, N. Zou, Novel square photonic crystal fibers with ultra-flattened chromatic dispersion and low confinement losses, *IEICE transactions on electronics* 90 (3) (2007) 607–612.
- [4] F. Begum, Y. Namihira, S. A. Razzak, S. Kaijage, N. H. Hai, T. Kinjo, K. Miyagi, N. Zou, Novel broadband dispersion compensating photonic crystal fibers: Applications in high-speed transmission systems, *Optics & Laser Technology* 41 (6) (2009) 679–686.
- [5] F. Begum, Y. Namihira, S. A. Razzak, S. Kaijage, N. H. Hai, T. Kinjo, K. Miyagi, N. Zou, Design and analysis of novel highly nonlinear photonic crystal fibers with ultra-flattened chromatic dispersion, *Optics communications* 282 (7) (2009) 1416–1421.
- [6] J. Joannopoulos, S. Johnson, J. Winn, R. Meade, *Photonic crystals: Molding the flow of light* 2nd edn princeton univ (2008).
- [7] G. Rajalakshmi, A. Sivanantha Raja, D. Shanmuga Sundar, Design and optimization of two dimensional photonic crystal based optical filter, *Journal of Nonlinear Optical Physics & Materials* 24 (03) (2015) 1550027.
- [8] P. Narmadhadevi, D. S. Sundar, L. Malathi, Performance analysis of different micro ring resonators based on optical delay lines, *International Journal of Computer Applications* 67 (13).
- [9] S. Geerthana, A. S. Raja, D. S. Sundar, Design and optimization of photonic crystal fiber with improved optical characteristics, *Journal of Nonlinear Optical Physics & Materials* 24 (04) (2015) 1550051.
- [10] M. Hasan, M. S. Habib, M. S. Habib, S. A. Razzak, Highly nonlinear and highly birefringent dispersion compensating photonic crystal fiber, *Optical Fiber Technology* 20 (1) (2014) 32–38.
- [11] J. Knight, T. Birks, P. S. J. Russell, D. Atkin, All-silica single-mode optical fiber with photonic crystal cladding, *Optics letters* 21 (19) (1996) 1547–1549.
- [12] J. Knight, T. Birks, R. Cregan, P. S. J. Russell, Large mode area photonic crystal fiber, *Optics and Photonics News* 9 (12) (1998) 34–35.
- [13] B. Bouma, M. Brezinski, J. Fujimoto, G. Tearney, S. Boppart, M. Hee, High-resolution optical coherence tomographic imaging using a mode-locked ti: Al<sub>2</sub>O<sub>3</sub> laser source, *Optics Letters* 20 (13) (1995) 1486–1488.
- [14] D. Chen, M.-L. Vincent Tse, H.-Y. Tam, Optical properties of photonic crystal fibers with a fiber core of arrays of subwavelength circular air holes: Birefringence and dispersion, *Progress In Electromagnetics Research* 105 (2010) 193–212.
- [15] Y. Sharma, R. Zafar, Ultra flattened dispersion over telecom wavelength in ring based photonic crystal fiber, *IOSR Journal of Electronics and Communication Engineering* 9 (2014) 11–14.
- [16] Y. Namihira, M. A. Hossain, J. Liu, T. Koga, T. Kinjo, Y. Hirako, F. Begum, S. Kaijage, S. Razzak, S. Nozaki, Dispersion flattened nonlinear square photonic crystal fiber for dental oct.
- [17] H. Ademgil, S. Haxha, Pcf based sensor with high sensitivity, high birefringence and low confinement losses for liquid analyte sensing applications, *Sensors* 15 (12) (2015) 31833–31842.
- [18] K. R. Priya, A. S. Raja, D. S. Sundar, Design of a dual-core liquid-filled photonic crystal fiber coupler and analysis of its optical characteristics, *Journal of Optical Technology* 83 (9) (2016) 569–573.
- [19] J. Knight, J. Arriaga, T. Birks, A. Ortigosa-Blanch, W. Wadsworth, P. S. J. Russell, Anomalous dispersion in photonic crystal fiber, *IEEE photonics technology letters* 12 (7) (2000) 807–809.
- [20] K. P. Hansen, Introduction to nonlinear photonic crystal fibers, *Journal of Optical and Fiber Communications Research* 2 (3) (2005) 226–254.
- [21] J. M. Dudley, J. R. Taylor, Ten years of nonlinear optics in photonic crystal fibre, *Nature Photonics* 3 (2) (2009) 85–90.
- [22] B. H. Lee, J. B. Eom, J. Kim, D. S. Moon, U.-C. Paek, G.-H. Yang, Photonic crystal fiber coupler, *Optics Letters* 27 (10) (2002) 812–814.
- [23] S. Kim, Y. S. Lee, C. G. Lee, Y. Jung, K. Oh, Hybrid square-lattice photonic crystal fiber with broadband single-mode operation, high birefringence, and normal dispersion, *Journal of the Optical Society of Korea* 19 (5) (2015) 449–455.
- [24] M. S. Islam, B. K. Paul, K. Ahmed, S. Asaduzzaman, M. I. Islam, S. Chowdhury, S. Sen, A. N. Bahar, Liquid-infiltrated photonic crystal fiber for sensing purpose: Design and analysis, *Alexandria Engineering Journal*.
- [25] F. Koohi-Kamali, M. Ebnali-Heidari, M. K. Moravvej-Farshi, Designing a dual-core photonic crystal fiber coupler by means of microfluidic infiltration, *International Journal of Optics and Photonics* 6 (2) (2012) 83–96.
- [26] K. R. Khan, T. X. Wu, Short pulse propagation in wavelength selective index-guided photonic crystal fiber coupler, *IEEE Journal of Selected Topics in Quantum Electronics* 14 (3) (2008) 752–757.
- [27] S. Lou, Z. Tang, L. Wang, Design and optimization of broadband and polarization-insensitive dual-core photonic crystal fiber coupler, *Applied optics* 50 (14) (2011) 2016–2023.

- [28] K. Saitoh, M. Koshiba, T. Hasegawa, E. Sasaoka, Chromatic dispersion control in photonic crystal fibers: application to ultra-flattened dispersion, *Optics Express* 11 (8) (2003) 843–852.
- [29] T.-L. Wu, C.-H. Chao, A novel ultraflattened dispersion photonic crystal fiber, *IEEE Photonics Technology Letters* 17 (1) (2005) 67–69.
- [30] M. Wandel, P. Kristensen, Fiber designs for high figure of merit and high slope dispersion compensating fibers, *Journal of Optical and Fiber Communications Reports* 3 (1) (2006) 25–60.